Biosensors and Bioelectronics 35 (2012) 456–460

Contents lists available at SciVerse ScienceDirect

Biosensors and Bioelectronics

journal homepage: www.elsevier.com/locate/bios

Short communication

Ultrasensitive and label-free detection of pathogenic avian influenza DNA by using CMOS impedimetric sensors

Wei-An Lai [b], Chih-Heng Lin [d], Yuh-Shyong Yang [d], Michael S.-C. Lu [a,b,c,*]

[a] Department of Electrical Engineering, National Tsing Hua University, Hsinchu 300, Taiwan, ROC
[b] Institute of Electronics Engineering, National Tsing Hua University, Hsinchu 300, Taiwan, ROC
[c] Institute of NanoEngineering and Microsystems, National Tsing Hua University, Hsinchu 300, Taiwan, ROC
[d] Department of Biological Science and Technology, National Chiao Tung University, Hsinchu 300, Taiwan, ROC

ARTICLE INFO

Article history:
Received 3 January 2012
Received in revised form 13 February 2012
Accepted 23 February 2012
Available online 3 March 2012

Keywords:
Avian influenza virus
Interdigitated microelectrode
CMOS
Integrated circuit

ABSTRACT

This work presents miniaturized CMOS (complementary metal oxide semiconductor) sensors for non-faradic impedimetric detection of AIV (avian influenza virus) oligonucleotides. The signal-to-noise ratio is significantly improved by monolithic sensor integration to reduce the effect of parasitic capacitances. The use of sub-μm interdigitated microelectrodes is also beneficial for promoting the signal coupling efficiency. Capacitance changes associated with surface modification, functionalization, and DNA hybridization were extracted from the measured frequency responses based on an equivalent-circuit model. Hybridization of the AIV H5 capture and target DNA probes produced a capacitance reduction of $-13.2 \pm 2.1\%$ for target DNA concentrations from 1 fM to 10 fM, while a capacitance increase was observed when H5 target DNA was replaced with non-complementary H7 target DNA. With the demonstrated superior sensing capabilities, this miniaturized CMOS sensing platform shows great potential for label-free point-of-care biosensing applications.

1. Introduction

Electrical bioassays hold great promise for numerous decentralized clinical applications ranging from emergency-room screening to point-of-care diagnostics due to their low cost, high sensitivity, specificity, speed, and portability. A miniaturized biosensing platform can be achieved through monolithic integration of sensing devices and detection circuits in an integrated-circuit process, such as the CMOS technology. Arrays of sensors fabricated on a CMOS chip can enhance sensing resolution and accuracy through statistical analysis of the collected data. CMOS biosensors have been implemented based on the electrochemical (Schienle et al., 2004), impedimetric (Lee et al., 2010), capacitive (Stagni et al., 2006; Lu et al., 2010), conductive (Li et al., 2003), ion-sensitive (Li et al., 2010), magnetic (Sun et al., 2009), optical (Eltoukhy et al., 2006), and micromechanical (Shekhawat et al., 2006) approaches. Some of the methods require labeling by using, for example, magnetic microbeads (Sun et al., 2009), and many are label-free for biosignal transduction. Sensing resolution at the fM level has been reported by using CMOS ion-sensitive field effect transistors (Li et al., 2010). The CMOS impedimetric sensors presented in this work are intended to demonstrate highly sensitive detection of AIV DNA.

Changes in the electrical properties of a sensing interface (e.g., capacitance, resistance) occur when a target biomolecule interacts with a probe-functionalized surface. An impedance change can be correlated to detection of DNA hybridization, antigen-antibody reaction, or biological cells. A conventional impedimetric biosensor measures the electrical impedance of an electrode-solution interface in a.c. steady state with constant d.c. bias conditions. This approach, known as electrochemical impedance spectroscopy (EIS), is accomplished by imposing a small sinusoidal voltage over a range of frequencies and measuring the resulting current. The impedance consists of both energy dissipation (resistor) and energy storage (capacitor) elements. In addition to the frequency-domain measuring method, interface impedance changes can be measured by the potentiostatic step method where small potential steps are applied to the working electrode and the transient current responses, as determined by the time constant of the interface resistance and capacitance, are measured accordingly. By this time-domain approach, a CMOS impedimetric sensor array (Lee et al., 2010) has achieved a sensing resolution of 10 nM for label-free DNA detection.

The faradaic EIS requires the addition of a redox species which is alternately oxidized and reduced by the transfer of charges to and from a metal electrode. In contrast, no additional reagent is required for non-faradaic impedance spectroscopy. The

* Corresponding author at: 101 Sec. 2 Kuang-Fu Rd., National Tsing Hua University, Department of Electrical Engineering, Hsinchu 30013, Taiwan, ROC.
Tel.: +1 886 3 516 2220; fax: +1 886 3 575 2120.
E-mail address: sclu@ee.nthu.edu.tw (M.S.-C. Lu).

0956-5663/$ – see front matter © 2012 Elsevier B.V. All rights reserved.
doi:10.1016/j.bios.2012.02.049

associated impedance change is predominantly capacitive (Hedström et al., 2005; Limbut et al., 2006; Loyprasert et al., 2008; de Vasconcelos et al., 2009; Qureshi et al., 2010) with the charge transfer resistance being omitted. The reported detection limits are generally between pg/ml to ng/ml. A low detection limit down to 7 fg/mL has been demonstrated by a microcystin-LR immunosensor (Loyprasert et al., 2008). Immobilization is a critical part in non-faradic impedimetric biosensors since the electrode surface has to be electrically insulated. This can be achieved by coating a dielectric thin film on electrode surface as in this work, or by using insulating self-assembled monolayers of sulfur compounds on gold electrodes (Berggren et al., 2001).

Avian influenza viruses, especially those highly pathogenic types (H5 and H7), are known to produce a significant morbidity rate and a mortality rate. All known viruses that cause influenza in birds belong to the species influenza *A* virus as most strains of all subtypes of influenza *A* virus are adapted to birds. Avian influenza viruses that cause diseases in both human and poultry are subtyped according to the antigenic subtype of the hemagglutinin (HA) and neuraminidase (NA) glycoproteins (e.g., H1N1). A pandemic may happen when a novel HA gene spreads rapidly among infected humans who do not have immunity to the virus. According to the report of World Health Organization in 2011, the total number of H5N1 human cases is 562 with 329 deaths. Therefore, development of highly sensitive, accurate, rapid, and cost-effective diagnostic tools is needed for surveillance programs as well as routine laboratory tests. For example, label-free AIV detection at fM level was reported by using functionalized poly-crystalline silicon nanowire field-effect transistors (Lin et al., 2009).

This study presents integrated CMOS impedimetric sensors for detection of the AIV H5 DNA. The impedance change is essentially capacitive due to a dielectric thin film on top of interdigitated microelectrodes for non-faradic detection. Signal transduction is achieved through a CMOS readout circuit. MOS transistors possess a high input impedance which is ideal for transducing the high-impedance bio-signals. Monolithic integration significantly promotes the signal-to-noise ratio by reducing the parasitic capacitances observed at the sensing node. The small gap (<μm) between interdigitated sensing electrodes also improves the sensing resolution by promoting signal coupling efficiency.

2. Materials and methods

2.1. Materials

3-Aminopropyltriethoxysilane (APTES) and ethanolamine were purchased from Sigma-Aldrich (USA). Glutaraldehyde in aqueous solution (25%) was purchased from Fluka (USA). AIV HA DNA sequences were designed based on prior works (Wang et al., 2008; Townsend et al., 2006). All synthetic oligonucleotides were purchased from MDBio Inc. (Taiwan) including 5′-aminomodified complementary AIV H5 capture DNA probe (5′-NH_2-CAA ATC TGC ATT GGT TAT CA-3′), 5′-Cyanine 3 (Cy3) modified target DNA (5′-Cy3-TGA TAA CCA ATG CAG ATT TG-3′), AIV H5 target DNA (5′-TGA TAA CCA ATG CAG ATT TG-3′), and AIV H7 target DNA (5′-TAC TCA ATT TGA CTG GGT CAA TTT G-3′). Phosphate buffer solution (PBS) was prepared in deionized (DI) water (pH = 7).

2.2. Surface functionalization and immobilization

The cross-sectional view in Fig. 1A illustrates the operating principle of impedimetric AIV H5 DNA detection. Interdigitated microelectrodes covered by the CMOS silicon dioxide thin film were utilized as the sensing interface to perform surface functionalization and immobilization. The CMOS sensors were firstly

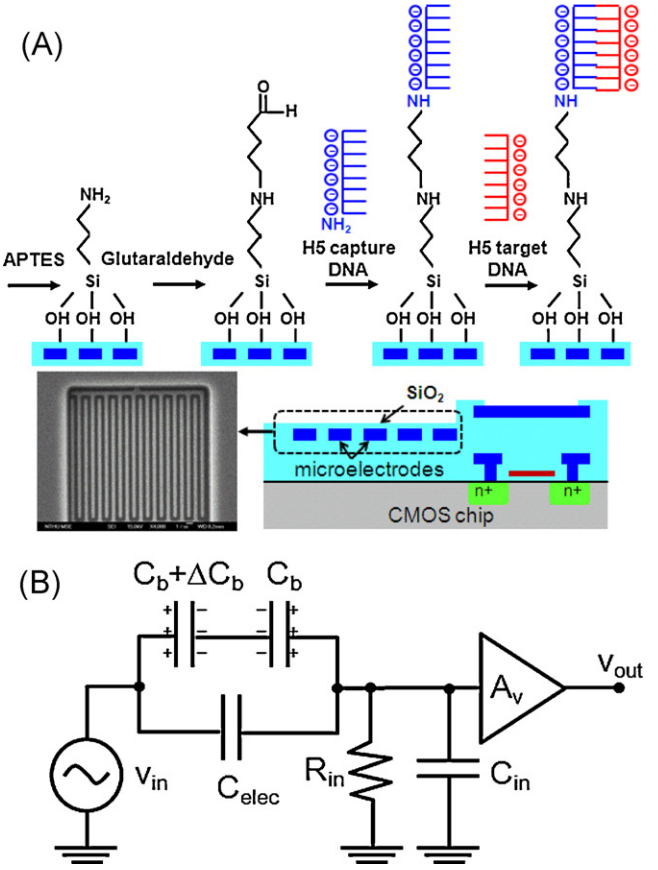

Fig. 1. (A) Surface modification and functionalization for impedimetric detection of AIV H5 DNA hybridization using CMOS interdigitated microelectrodes. The scanning electron micrograph shows the top view of the electrodes. (B) The equivalent-circuit model for impedimetric detection.

washed by ethanol and acetone solutions for 10 min respectively to remove contaminants and introduce–OH on the oxide surface before they were immersed in 2% APTES ethanol solution for 30 min to introduce amino groups on the oxide surface. The devices were then washed with ethanol (99.5%) for three times. In the following step, the device surface was immersed in solution containing 2.5% glutaraldehyde in 10 mM PBS (pH = 7.0) for 2 h to produce aldehyde groups, and then washed by PBS. Finally, the 10-μM 5′-aminomodified capture DNA probes mixed in 10-mM PBS were immobilized on the sensor surface after 10 h. The un-reacted aldehyde groups were blocked by mixing with 50-mM ethanolamine and 4-mM sodium cyanoborohydride in 10-mM PBS for 30 min.

2.3. Device fabrication

A two-polysilicon-four-metal (2P4M) 0.35-μm CMOS process was used for sensor fabrication. The CMOS aluminum layer (metal-3) was used as the electrode material and the inter-metal silicon dioxide on metal-3 was used for immobilization of the DNA capture probes. The passivation thin films on top of microelectrodes were removed by dry etch in the foundry. The remaining oxide thickness on the metal-3 electrodes was 0.35 μm as measured by a surface profilometer (Kosaka ET4000a). A thin silicon dioxide is desired in this study to promote the signal-coupling efficiency. The area of interdigitated microelectrodes is $20 \times 20\ \mu m^2$. The electrode length, thickness, separation, and width are 18, 0.64, 0.5, and 0.6 μm, respectively. The thickness of silicon dioxide beneath microelectrodes is 4.4 μm. The electrode capacitance is calculated

by finite-element simulation to be 40 fF. Scanning electron micrograph of the interdigitated microelectrodes is also shown in Fig. 1A.

2.4. Sensing circuit

As depicted by the equivalent-circuit model in Fig. 1B, the sensor mainly consists of the interdigitated microelectrodes C_{elec}, the electrode-analyte interface capacitance C_b, and a buffer amplifier for readout. The charge transfer resistance is omitted from our model since there is no electrochemical current flowing between the electrodes covered by silicon oxide. The solution resistance is also neglected since it is much less than the interface capacitive. The frequency response of each sensor is defined as the ratio of sensor output over input, which is obtained by applying a sinusoidal input over a range of frequencies to one side of the interdigitated microelectrodes and measuring the corresponding circuit output. The interface capacitance change, denoted as ΔC_b, is produced due to an electrostatic force induced by the sinusoidal input. The signal change due to ΔC_b is enhanced by electrodes with a sub-μm gap. The pre-amp input resistance and capacitance are represented by R_{in} and C_{in}, respectively. The ratio of the sensor output over input represented in Laplace transform is given by:

$$\frac{v_o(s)}{v_i(s)} = A_v \cdot \frac{sR_{in}(C_{elec} + \Delta C_b)}{1 + sR_{in}(C_{in} + C_{elec} + \Delta C_b)} \quad (1)$$

The buffer amplifier contains a source follower circuit made of p-type transistors. The circuit intends to provide a moderate input capacitance to enhance the output signal while reducing the flicker noise. A n-type MOS transistor operated in the sub-threshold region is used to implement a large resistance for R_{in}, which forms a high-pass frequency response with the associated capacitances. The drain terminal of the sub-threshold transistor is connected to one side of the microelectrodes. This high-pass corner frequency can be varied due to the change of R_{in} influenced by the dipole potential on sensor surface.

Fig. S1 in the Supplementary information shows the measured frequency responses (in air) of four sensors on a CMOS chip by using a spectrum/network analyzer (Agilent 4395A). The input capacitances (C_{in}) of the four sensors on the chip were extracted to be 32 ± 2 fF based on the measured mid-band gains and the electrode capacitance. The input resistances R_{in} were also extracted to be 28.5 ± 1.5 MΩ based on the measured corner frequencies. The measured C_{in} and R_{in} values are quite consistent across chips; for example, the values measured from one of the other chips were 32.4 ± 0.6 fF and 23.8 ± 0.7 MΩ, respectively.

3. Results and discussions

3.1. Fluorescence detection of DNA hybridization

The H5 capture DNA was synthesized via a series of chemical reactions as depicted in Fig. 1A. 5′-Cy3 modified H5 target DNA was used as the fluorescent reporter to identify immobilized H5 capture DNA on silicon dioxide surface. As shown in the Supplementary Information, clear distinction in fluorescence was observed between Fig. S2A and B for the cases with and without H5 capture DNA. Two other control experiments without adding APTES and glutaraldehyde, respectively, were also performed and fluorescence was not observed in both cases. Only the device following all steps gave the expected fluorescent upon hybridization with 5′-Cy3 modified H5 target DNA under green light excitation.

3.2. Characterization of surface modification and functionalization processes

The frequency responses of four sensors on the chip were measured before and after adding APTES, glutaraldehyde, 5′-aminomodified H5 capture DNA, and ethanolamine. Sensors immersed in the buffer solution were measured before each step. The solution potential was provided by an Ag/AgCl reference electrode biased at the same ground potential as the CMOS chip for all measurements. Fig. 2A–D show the measured frequency responses from one of the sensors before and after each step. The associated capacitance and resistance changes before and after each step were analyzed using the equivalent circuit in Fig. 1B. The percentage capacitance changes in ΔC_b were $18.6 \pm 6.9\%$, $-31.8 \pm 3.2\%$, $-27.8 \pm 3.4\%$, and $80.7 \pm 4.6\%$, respectively, after each step. The percentage capacitance changes in R_{in} were $53.3 \pm 2.2\%$, $-0.2 \pm 0.2\%$, $-13.6 \pm 3\%$, and $79.0 \pm 33.5\%$, respectively, after each step. A capacitance increase or decrease is associated with electrical charges and/or a dielectric property change at the electrode-analyte interface. The capacitance increase after adding APTES could be partially owing to the fact that the amino group ($pK_a > 9$) was protonated to $-NH_3^+$. The capacitance decrease after adding the electrically neutral glutaraldehyde could be due to a dielectric property change at the interface. A capacitance decrease was observed after immobilization of the H5 capture DNA probes with negative charges. The capacitance increase after adding ethanolamine with sodium cyanoborohydride could be owing to the fact that the remaining free aldehyde groups formed amine groups that exhibited positive charges in a neutral buffer.

3.3. H5 target DNA detection

H5 target DNA and H7 target DNA prepared in PBS buffer were added on separate CMOS chips immobilized with H5 capture DNA. The frequency responses of all four sensors on the two chips during hybridization were measured for target DNA concentrations from 1 fM to 1 nM. The measured mid-band gains for the experiment (H5–H5) and control (H5–H7) groups decreased and increased, respectively, under increasing target DNA concentrations as shown in Fig. S3A and B. As shown in Fig. S3B, the gain measured at 1 nM was lower than the gain at 1 fM for frequencies higher than 80 kHz. The reason was that the capacitive loading of the sensing circuit increased as the interface capacitance on chip surface increased, resulting in a reduced −3 dB frequency. As depicted in Fig. 3, the extracted capacitance ΔC_b resulting from H5–H5 and H5–H7 hybridization processes decreased and increased, respectively, with respect to the target DNA concentration. The reduction and increase in ΔC_b could be associated with the negative DNA charges and the dielectric property change at the interface, respectively. The ΔC_b values after adding 1-fM H5 and 1-fM H7 target DNA probes were 0.437 ± 0.054 pF and 0.204 ± 0.031 pF, respectively. The percentage changes for H5–H5 binding from 1 fM to 10 fM was $-13.2 \pm 2.1\%$, indicating that our CMOS impedimetric sensors can achieve highly sensitive AIV detection at the fM level (i.e., 6.14 fg/ml). This result is comparable to the AIV measurement using nanowire field-effect transistors (Lin et al., 2009). A comparison of the detection limit to prior works is summarized in Table S1 (Kukol et al., 2008; Pavlovic et al., 2008; Ting et al., 2009). The sensing resolution of our integrated, non-faradic detection method is comparable to or better than those reported by using the conventional faradic approach.

It is beneficial to use statistical data collected from multiple sensors on the same chip to understand sensor's repeatability and detection limit. As shown in Fig. S4, similar capacitance changes and femto-molar resolution were also observed in a repeated experiment.

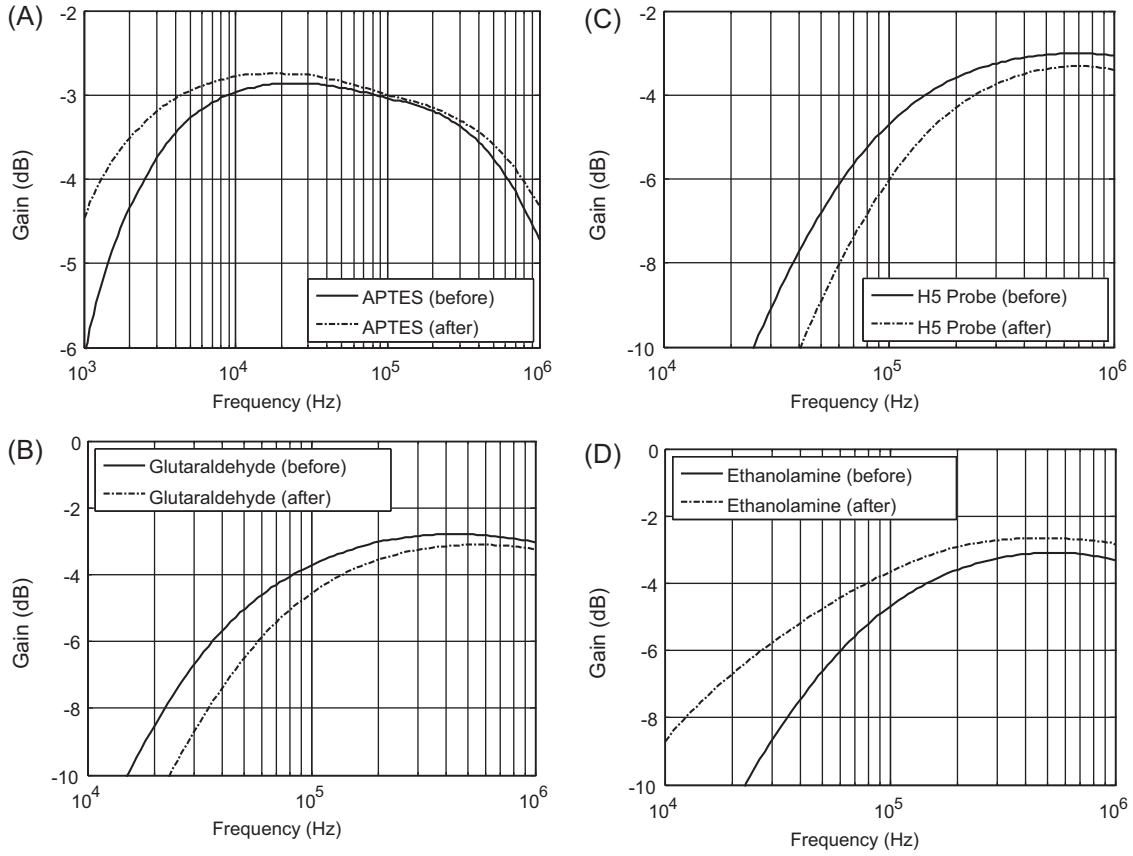

Fig. 2. Measured frequency responses of one of the sensors before and after adding: (A) APTES, (B) glutaraldehyde, (C) 5′-aminomodified H5 capture DNA, and (D) ethanolamine.

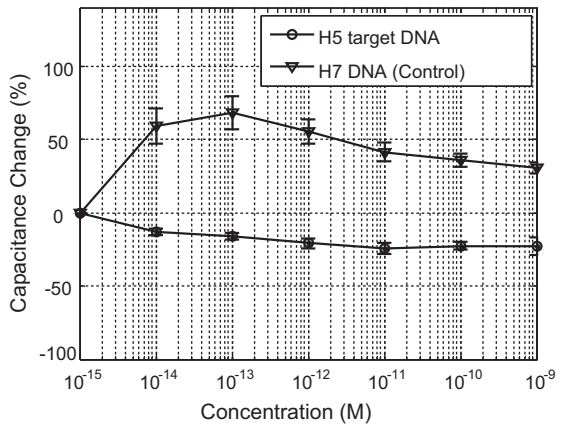

Fig. 3. Percentage capacitance changes of CMOS impedimetric sensors after hybridization with H5 and H7 target DNA probes, respectively, under increasing concentrations.

4. Conclusions

Non-faradic impedimetric detection of AIV DNA in the fM range has been demonstrated in this work by using sub-μm CMOS interdigitated microelectrodes as the sensing interface. Signal coupling efficiency and sensitivity are enhanced by monolithic integration, and can be further improved with the scaling of CMOS technologies. The proposed sensor fabrication requires no additional lithographic steps after the conventional CMOS processes, and the CMOS dielectric thin film can be conveniently used for DNA immobilization. This CMOS biosensing platform provides great potential for portable biosensing applications that require real-time, label-free, and ultrasensitive detection.

Acknowledgement

The project is supported by the National Science Council, Taiwan. We are very grateful to the National Chip Implementation Center for support of chip fabrication and the National Center for High-Performance Computing for support of simulation tools.

Appendix A. Supplementary data

Supplementary data associated with this article can be found, in the online version, at doi:10.1016/j.bios.2012.02.049.

References

Berggren, C., Bjarnason, B., Johansson, G., 2001. Electroanalysis 13, 173–180.
de Vasconcelos, E.A., Peres, N.G., Pereira, C.O., da Silva, V.L., da Silva Jr., E.F., Dutra, R.F., 2009. Biosens. Bioelectron. 25, 870–876.
Eltoukhy, H., Salama, K., El Gamal, A., 2006. IEEE J. Solid-State Circuits 41, 651–662.
Hedström, M., Galaev, I.Y., Mattiasson, B., 2005. Biosens. Bioelectron. 21, 41–48.
Kukol, A., Li, P., Estrela, P., Ko-Ferrigno, P., Migliorato, P., 2008. Anal. Biochem. 374, 143–153.
Lee, K., Lee, J., Sohn, M., Lee, B., Choi, S., Kim, S.K., Yoon, J., Cho, G., 2010. Biosens. Bioelectron. 26, 1373–1379.
Li, D.C., Yang, P.H., Lu, M.S.-C., 2010. IEEE Trans. Electron Devices 57, 2761–2767.
Li, J., Xue, M., Lu, Z., Zhang, Z., Feng, C., Chan, M., 2003. IEEE Trans. Electron Devices 50, 2165–2170.
Limbut, W., Kanatharana, P., Mattiasson, B., Asawatreratanakul, P., Thavarungkul, P., 2006. Biosens. Bioelectron. 22, 233–240.
Lin, C.H., Hung, C.H., Hsiao, C.Y., Lin, H.C., Ko, F.H., Yang, Y.S., 2009. Biosens. Bioelectron. 24, 3019–3024.
Loyprasert, S., Thavarungkul, P., Asawatreratanakul, P., Wongkittisuksa, B., Limsakul, C., Kanatharana, P., 2008. Biosens. Bioelectron. 24, 78–86.
Lu, M.S.-C., Chen, Y.C., Huang, P.C., 2010. Biosens. Bioelectron. 26, 1093–1097.

Pavlovic, E., Lai, R.Y., Wu, T.T., Ferguson, B.S., Sun, R., Plaxco, K.W., Soh, H.T., 2008. Langmuir 24, 1102–1107.
Qureshi, A., Niazi, J.H., Kallempudi, S., Gurbuz, Y., 2010. Biosens. Bioelectron. 25, 2318–2323.
Schienle, M., Paulus, C., Frey, A., Hofmann, F., Holzapfl, B., Schindler-Bauer, P., Thewes, R., 2004. IEEE J. Solid-State Circuits 39, 2438–2445.
Shekhawat, G., Tark, S.H., Dravid, V.P., 2006. Science 311, 1592–1595.
Stagni, C., Guiducci, C., Benini, L., Ricco, B., Carrara, S., Samori, B., Paulus, C., Schienle, M., Augustyniak, M., Thewes, R., 2006. IEEE J. Solid-State Circuits 41, 2956–2963.
Sun, N., Liu, Y., Lee, H., Weissleder, R., Ham, D., 2009. IEEE J. Solid-State Circuits 44, 1629–1643.
Ting, B.P., Zhang, J., Gao, Z.Q., Ying, J.Y., 2009. Biosens. Bioelectron. 25, 282–287.
Townsend, M.B., Dawson, E.D., Mehlmann, M., Smagala, J.A., Dankbar, D.M., Moore, C.L., Smith, C.B., Cox, N.J., Kuchta, R.D., Rowlen, K.L., 2006. J. Clin. Microbiol. 44, 2863–2871.
Wang, L.C., Pan, C.H., Severinghaus, L.L., Liu, L.Y., Chen, C.T., Pu, C.E., Huang, D., Lir, J.T., Chin, S.C., Cheng, M.C., Lee, S.H., Wang, C.H., 2008. Vet. Microbiol. 127, 217–226.